Available online at www.sciencedirect.com
ScienceDirect
Journal of Structural Biology 157 (2007) 393–402
Journal of Structural Biology
www.elsevier.com/locate/yjsbi

Crystallographic structure of the foliated calcite of bivalves

Antonio G. Checa [a,*], Francisco J. Esteban-Delgado [a], Alejandro B. Rodríguez-Navarro [b]

[a] Departamento de Estratigrafía y Paleontología, Facultad de Ciencias, Universidad de Granada, Avenida Fuentenueva s/n, 18071 Granada, Spain
[b] Departamento de Mineralogía y Petrología, Facultad de Ciencias, Universidad de Granada, Avenida Fuentenueva s/n, 18071 Granada, Spain

Received 9 May 2006; received in revised form 22 September 2006; accepted 24 September 2006
Available online 11 October 2006

Abstract

The foliated layer of bivalves is constituted by platy calcite crystals, or laths, surrounded by an organic layer, and which are arranged into sheets (folia). Therefore, the foliated microstructure can be considered the calcitic analogue to nacre. In this paper, the foliated microstructure has been studied in detail using electron and X-ray diffraction techniques, together with SEM observations on naturally decalcified shells, to investigate the crystallographic organization on different length scales and to resolve among previous contradictory results. This layer is highly organized and displays a coherent crystallographic orientation. The surface of the laths of the foliated layer is constituted by calcite crystals oriented with their *c*-axis tilted opposite to the growth direction of the laths and one of its $\{10\bar{1}4\}$ rhombohedral faces looking in the growth direction. These faces are only expressed as the terminal faces of the laths, whereas the main surfaces of laths coincide with $\{10\bar{1}8\}$ rhombohedral faces. This arrangement was consistently found in all specimens studied, which leads us to the provisional conclusion that, unlike previous studies, there is only one possible crystallographic arrangement for the foliated layer. Future studies on other species will help to ascertain this assertion.

Keywords: Biomineralisation; Microstructure; Shell; Calcite; Foliated layer; Bivalves; Oysters; Scallops; Electron back scattering diffraction; X-ray diffraction

1. Introduction

Foliated microstructure is defined as being composed of blade-like elongate parallel crystals (laths) of calcite with arrow-point endings which coalesce laterally forming laminae (folia) (Fig. 1). The folia dip uniformly over large areas and usually reach the surface of secretion of the shell at a reduced angle. Clear descriptions of the morphology and mode of growth of the foliated layer can be found in Taylor et al. (1969) and Carter (1980).

The foliated layer is particularly frequent in bivalves, where it forms the bulk of the shells of several epibenthic groups (Table 1). It is present in the Middle Cambrian bivalve *Tuarangia* (MacKinnon, 1982; Runnegar, 1985; Berg-Madsen, 1987), but it does not reappear until the Upper Devonian (in the pectinoid genus *Saharopteria*, e.g., Carter, 1990), from whence it has been increasingly frequent in bivalves.

The typical foliated fabric is also found in some limpets (e.g., Carter and Hall, 1990). Outside the Mollusca, it has been described in cyclostome bryozoans (Taylor and Weedon, 2000) and a similar microstructure (the calcitic cross-bladed lamination; see, e.g., Williams, 1997) also occurs in some articulate brachiopods.

The foliated microstructure has been studied by many authors (see introduction in Runnegar, 1984), but only a few have described the crystallographic orientation of crystals in this microstructure. Fig. 2 summarizes the basic information regarding crystal orientation and the techniques used in previous studies. It can be observed that crystallographic orientations reported by different authors vary substantially and are clearly in conflict with each other. Among these studies, the most comprehensive is that of Runnegar (1984), which comprises several families. This

* Corresponding author. Fax: +34 958 248528.
E-mail address: acheca@ugr.es (A.G. Checa).

1047-8477/$ - see front matter © 2006 Elsevier Inc. All rights reserved.
doi:10.1016/j.jsb.2006.09.005

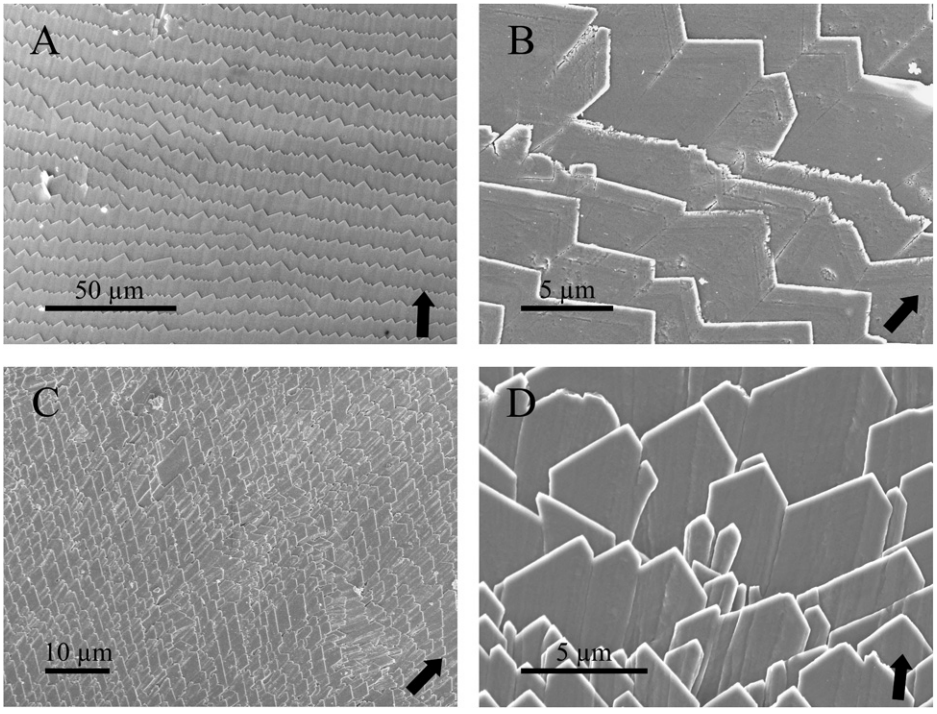

Fig. 1. Surface views of the foliated layers of *A. ephippium* (A and B) and *O. edulis* (C and D) showing the different degrees of coplanarity of laths and development of folia. Arrows indicate growth direction of the shell.

Table 1
Bivalve families with foliated layers

Order Ostreoida
Superfamily Ostreoidea: families Ostreidae*, Gryphaeidae
Superfamily Pectinoidea: families Pectinidae*, Propeamussiidae*, Spondylidae
Superfamily Anomioidea: families Anomiidae*, Placunidae*
Order Limoida
Superfamily Limoidea: family Limidae

Asterisks indicate the groups studied.

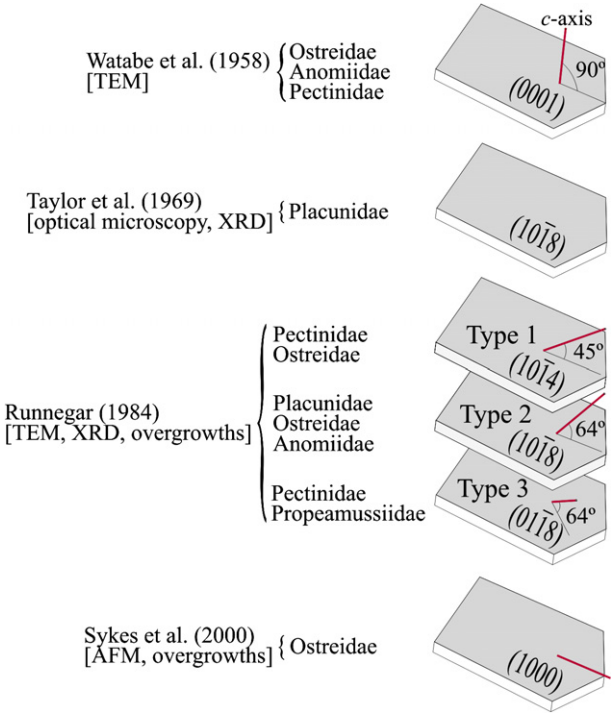

Fig. 2. Interpretations of the crystallography of the foliated layers in previous studies (see above-mentioned references for further information).

author proposes more than one solution within single families (*Ostreidae* and *Pectinidae*) and even species (*Crassostrea virginica*). This uncertainty could be due either to: (1) a high variability of the crystallographic properties of such microstructures or (2) ambiguity in the determination of the crystallographic orientation resulting from the techniques used. The first possibility is not likely since organisms displaying this microstructure type (i.e., bivalves) are known to control the orientation and disposition of crystals. This control is exerted by different, genetically defined factors and results in highly reproducible microstructural characteristics displayed by organisms belonging to the same group (Addadi and Weiner, 1992). Regarding the second possibility, previous authors have determined crystal orientation using XRD, TEM, and other types of microscopy (OM, AFM). Crystal orientation cannot be precisely and unambiguously determined based on morphology alone obtained by optical, scanning electron or atomic force microscopy. TEM provides much more precise information about crystal orientation of a thin sectioned sample by means of selected area electron diffraction (SAED). Nevertheless, SAED patterns obtained are sections of the reciprocal space and in order to define the disposition of the main crystallographic axes, the sample needs to be cut and oriented adequately (Beeston et al., 1986). Further-

more, SAED patterns are from a very small sample area (~0.5 μm in diameter) and only provide information about the orientation of individual crystals and not about the long range order of crystals in the shell. Conventional θ–2θ scans determined by XRD give only limited information about the preferential orientation of crystals (Rodríguez-Navarro et al., 2002). To determine the three-dimensional crystallographic orientation, other techniques are available, including XRD texture analysis and electron back scatter diffraction (EBSD). These techniques provide much more detailed and unambiguous information of the 3-D disposition of crystals than do the previously mentioned techniques. They provide the distribution of pole densities of crystallographic directions needed to define the orientation of crystals. Additionally, these two techniques are complementary and give high resolution information about the organization of crystals on different scales from millimeters (XRD texture analysis) to micrometers (EBSD). While the first technique gives statistical information of the disposition of crystals in the shell, the second yields detailed local information about the orientation of individual crystals. XRD texture analysis has been applied to study different shell microstructure types (see Chateigner et al., 2000, and references therein) but not the foliated microstructure. Our study has been based mainly on the above mentioned two techniques.

The crystallographic structure is a basic ultrastructural aspect and is a prerequisite for further studies dealing with morphogenetic, evolutionary-systematic and, even, biomimetic aspects. Our study aims to determine the main crystallographic directions of crystals of the foliated layer and whether there is more than one crystallographic arrangement.

2. Materials and methods

2.1. Materials

The following species have been investigated: the oysters *Ostrea edulis* Linnaeus, 1758, *Ostrea puelchana* D'Orbigny, 1842 and *Crassostrea gigas* (Thunberg, 1873) (Ostreidae), the scallops *Pecten maximus* Linnaeus, 1758, *Aequipecten opercularis* (Linnaeus, 1758), *Mimachlamys varia* (Linnaeus, 1758) (Pectinidae), *Adamussium colbecki* (Smith, 1902), *Propeamussium jeffreysi* (Smith, 1885) and *Propeamussium sibogai* (Dautzenberg and Bavay, 1904) (Propeamussiidae), the window-pane shell *Placuna placenta* (Linnaeus, 1758) (Placunidae), and the saddle shell *Anomia ephippium* (Linnaeus, 1758) (Anomiidae). Except for *O. puelchana, A. colbecki, Pr. sibogai*, *Pr. jeffreysi*, and *P. placenta*, we always observed shells of freshly killed animals (caught in the Mediterranean coast of Andalucía, Spain). Specimens of *M. varia*, *P. maximus* and *A. ephippium* were kept alive for some two weeks in aquaria. Probably due to the shortage of food, the interior of the valves showed a delicate dissolution of the constituent crystallites and their organic envelopes, which revealed its ultrastructure.

2.2. Scanning electron microscopy

SEM observation of nacre crystals was carried out both in fractured specimens and in the shell interiors. Samples were usually observed intact, although in some we removed either the organic [with 5% NaOH for one to two hours or proteinase K (1 mg ml^{-1}) from 1 to 20 min] or mineral matter (2–4% EDTA) at room temperature. Samples were coated either with carbon (UHS evaporator, Hitachi, Japan) for FESEM observation (Gemini 1530, Leo, Germany) and Ultra-high resolution FESEM (S-5200, Hitachi, Japan).

2.3. X-ray diffraction

The three-dimensional orientation of the shell crystals was determined using an X-ray single diffractometer equipped with an area detector (D8 SMART APEX, Bruker, Germany). For diffraction experiments, the working conditions were: Mo Kα, 50 KV and 30 mA, a pin-hole collimator of 0.5 mm in diameter, and an exposure time of 20 s per frame. Shell samples were measured by reflection (diffractometer ω and 2θ angles were set at 10 and 20°, respectively) without polishing the surface. A set of frames (2-D diffraction patterns) was registered while rotating the sample around ϕ angle (a frame every degree; a total of 180 frames). Pole densities for the strongest calcite reflections (102, 104, 006, 110, 113, 202, 018, and 116) were calculated using XRD2DScan software (www.ugr.es/~anava/xrd2dscan.htm) and displayed in stereographic projection using specially designed visualization software. Each pole figure displays the intensity variation of a given hkl reflection as a function of the sample orientation (Fig. 3). From these plots, the 3-D orientation of associated {hkl} crystal faces can be observed. Pole figures calculated in this way were compared to those measured using a conventional X-ray texture diffractometer (D-5000, Siemens, Germany).

Pole figures were registered for *O. edulis*, *O. puelchana*, *P. maximus*, *M. varia*, *A. colbecki*, *Pr. sibogai*, *P. placenta*, and *A. ephippium* shells.

2.4. Electron diffraction

The electron back scatter diffraction (EBSD) technique analyzes the diffraction pattern produced when backscattered electrons are diffracted by a crystalline material. This pattern provides information about the orientation of the crystal lattice and the space group of the crystal structure (Randle, 2000). Using the scanning capabilities of a SEM (XL-30, Philips, The Netherlands), data from different positions can be either integrated into an orientation map or processed to obtain pole figures, pole plots or rocking curves resembling those obtained by X-ray diffraction. We have used the same system of representation (stereographic projection) as for XRD data. This technique provides resolution on a μm scale and is therefore a good complement to the broader scale, X-ray-based techniques

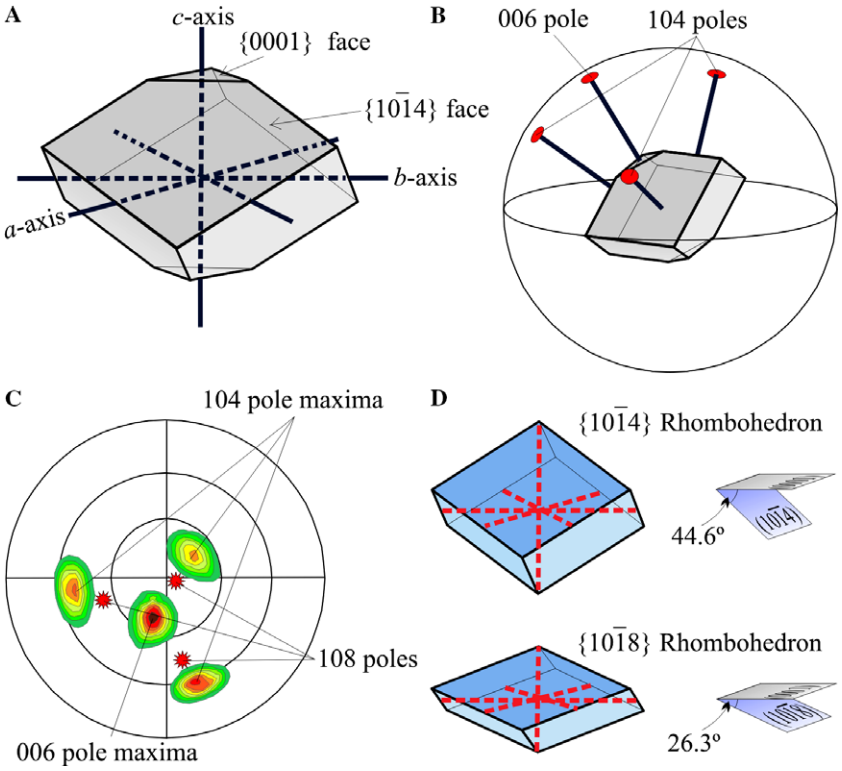

Fig. 3. (A) Schematic drawing of a calcite crystal displaying the spatial arrangement of their main crystal faces, their associated Miller–Bravais indexes and its crystallographic axes. (B) Relative orientation of 001 and 104 poles associated to a {0001} face and three {10$\bar{1}$4} rhombohedral faces. The three {10$\bar{1}$4} faces in the positive part of the *c*-axis are related by a three fold rotation axis parallel to the *c*-axis (or ⟨00.1⟩ pole). (C) Stereographic projection showing the usual aspect of 006 and 104 pole densities in an ordered material. The estimated position of ⟨10*8⟩ poles is also shown. This disposition of maxima indicates that calcite crystals are biaxially aligned. (D) Interfacial angle between {0001} and both {10$\bar{1}$4} and {10$\bar{1}$8}.

also used. Details about the EBSD technique can be found in, e.g., Randle and Engler (2000).

Measurements were made on the inner surface close to the shell margin of *O. edulis*, *P. placenta*, and *A. ephippium*, making sure that the foliated layer was clearly exposed. Samples were analyzed unpolished and only the organic matter was removed from the samples prior to analysis. We measured areas of 25×25 μm and a step size of 0.5 μm was selected. Despite the absence of any conductive coating, no excessive charging of the specimens was observed and the quality of the patterns was acceptable in almost all cases.

3. Results

3.1. SEM observations

As has been described, folia are composed by adjacent, blade-like laths. The degree of coplanarity of laths and hence the lateral extension of folia varies for different species (Fig. 1). Laths are typically 2–5 μm wide (Fig. 1B and D) and 200–250 nm thick (Fig. 4A) and have arrow point endings, which are sometimes truncated (Figs. 1B and D, 4B–D). The surface of laths shows growth lines produced by the advance of their growth fronts (Figs. 1B and 4C). New laths appear either as outgrowths of pre-existing laths (dendritic growth; Watabe and Wilbur, 1961) (Fig. 4D) or, more rarely, by epitaxial nucleation on the surface of previous crystals (Fig. 4E). On the shell internal surface each folium emerges from below at a low angle (usually 2–3°), although there are notable exceptions. For example, in the area close to the shell border of oysters, where the shell thickens rapidly and forms a wide wedge, folia meet the secretion surface at angles of 30° or greater. Folia tend to grow in the direction of shell growth, though this direction may vary over specific areas of the shell (Fig. 4F).

Specimens of *O. edulis* frequently cease to secrete carbonate in particular areas of the shell interior, while organic matter continues to be produced. These areas have a greenish, slightly translucent aspect and stand out on the white foliated background. The transition from the organic layer to the foliated layer is progressive. Sparse, disoriented grains composed of the same material as the normal foliated layer first settle onto the organic layer (Fig. 5). In transverse section, they have a spherulithic appearance. Their density increases progressively until they coalesce. The strictly foliated layer begins when the aggregate finally achieves a common orientation (Fig. 5).

In aquarium specimens of *Chlamys varia*, *P. maximus* and *A. ephippium*, naturally corroded shells show that laths of the foliated layer have a continuous organic coating and a substructure of tiny rhombohedra, which are evenly ori-

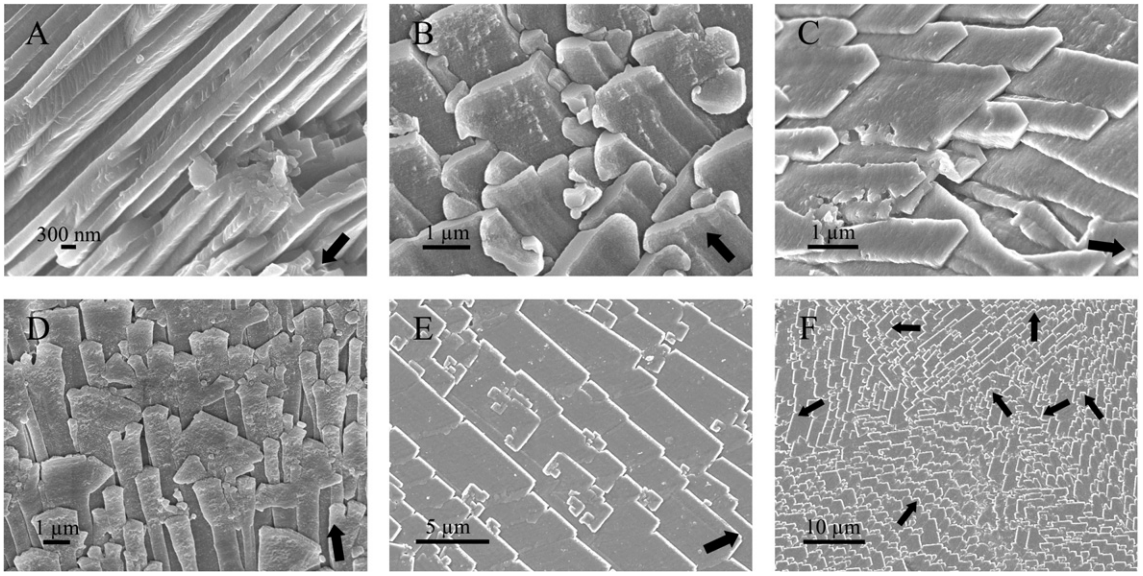

Fig. 4. (A) Cross sectional view of the foliated layer of *O. edulis*. (B) Terminal faces of laths in *C. varia*, some of which can be interpreted as $\{10\bar{1}4\}$ rhombohedral faces. (C) Terminal $\{10\bar{1}4\}$ faces in the foliated layer of *Propeamussium dalli*. (D) Dendritic growth of laths in the foliated layer of *C. varia*. (E) Epitaxial nucleation of new laths in the foliated layer of *O. edulis*. (F) Differently oriented sets of folia in *O. edulis*. Arrows indicate the growth direction of the folia.

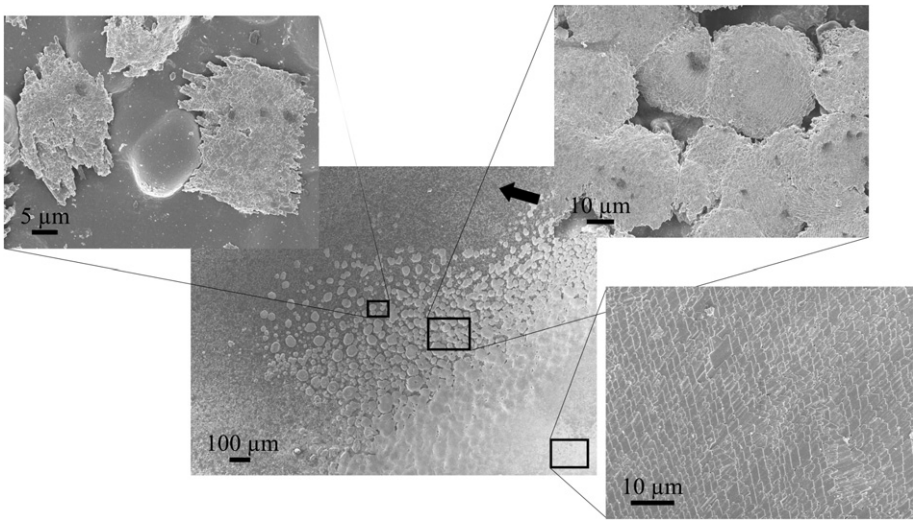

Fig. 5. Transition between an organic layer (dark area in the center micrograph) and the normal foliated layer (white area) on the internal shell surface of *O. edulis*. The process of calcification progresses towards the right bottom side. It initiates with the deposition of isolated and disoriented foliated grains (upper left micrograph); background bulges are calcite rhombohedra formed within the organic layer. When the density and size of grains increases they begin to interact with each other although the whole is highly disoriented (upper right micrograph). The material becomes highly organized shortly after carpeting of the organic surface is completed (lower right micrograph).

ented and also co-oriented with those of neighbouring laths and folia (Fig. 6A and B). The orientation of corrosion rhombohedra is consistent in the three species examined and there is always a rhombohedral face (the one which is the best exposed in plan view) looking in the direction of growth while the other two are looking backwards. In lateral view, the face looking forwards is less inclined with respect to the lath surface than the edge of the faces looking backward. Their outlines form an angle greater than 90° (Fig. 6C).

3.2. X-ray and electron diffraction

Pole figures determined either by XRD or EBSD in the different shells analysed are always consistent, so we will refer to them without distinction. A selection of samples is shown in Figs. 7 and 8. We should stress that 006 and 001 pole figures determined by XRD and EBSD, respectively, represent the orientation of $\{0001\}$ crystal planes of calcite and are equivalent. In all specimens studied, the 006/001 pole figures display one single maxima at a vari-

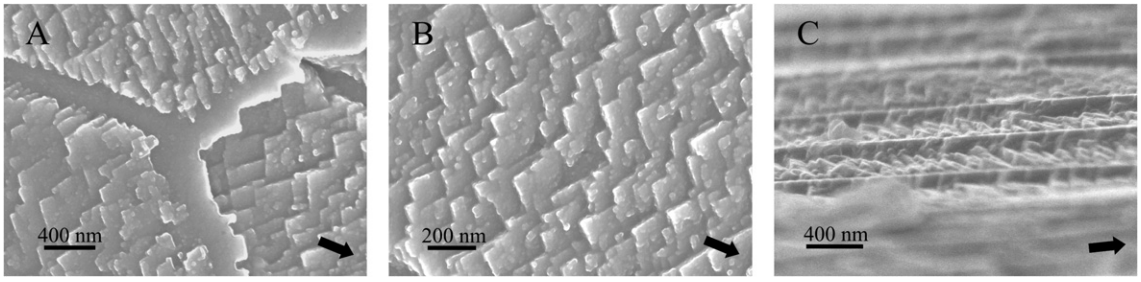

Fig. 6. (A,B) Internal surface of a naturally corroded shell of *A. ephippium*, showing the substructure consisting of aligned $\{10\bar{1}4\}$ rhombohedra. (C) Lateral view of corroded folia of *A. ephippium*.

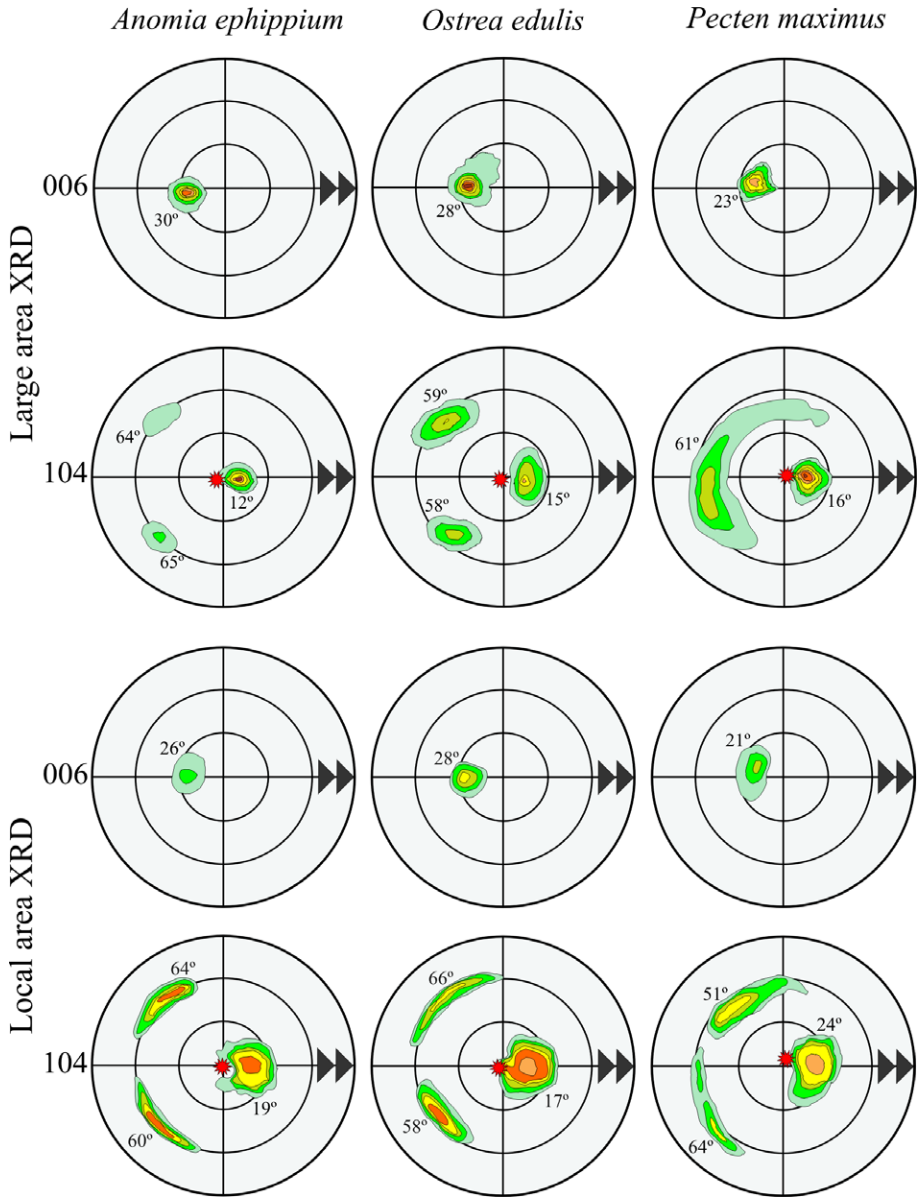

Fig. 7. Pole figures determined by standard or large area (~5 × 5 mm) and local area (0.5 × 0.5 mm) X-ray diffraction texture analysis for the calcitic foliated layer of different species. The 006 pole figures display a unique maximum placed at a slightly variable angular distance of the center (indicated in the figure) implying that crystals are oriented with their *c*-axis co-aligned and tilted relative to the shell normal. The 104 pole figures display three well defined maxima, which shows that crystals are biaxially oriented. The exception is the standard pole figure of *P. maximus* that has a ring-like disposition, due to an incipient turbostratic distribution of crystals. Numbers within figures refer to the angular distances from the centers of pole maxima to the center of the pole figure. The estimated positions of the ⟨10.8⟩ poles (✹) and the growth direction of the shells (⏩) are also indicated.

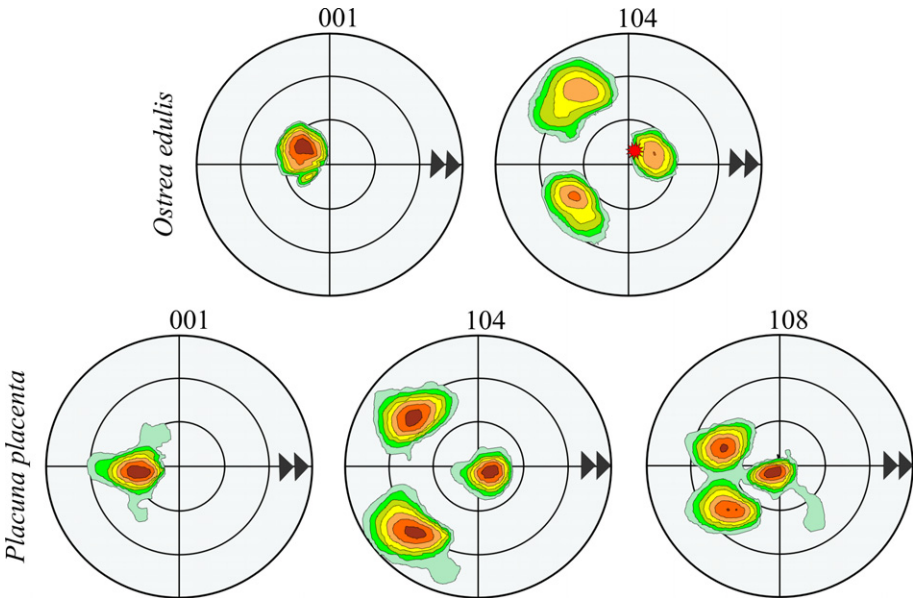

Fig. 8. Pole figures from single folia determined by EBSD for *O. edulis* and *P. placenta*, showing the orientation of crystals relative to the growth direction. Note that there is always a $\{10\bar{1}4\}$ rhombohedral face oriented in the growth direction and that the *c*-axis is tilted backward relative to the shell growth direction. The 108 pole figure of *P. placenta* is intended to show the almost coincidence of one 108 pole maxima with the center of the pole figure. The estimated position of the $\langle 10.8\rangle$ pole (✷) and the growth direction of the folia (▸▸) are indicated.

able angular distance from the center (between 21° and 30°. On the other hand, the 104 pole figures display three well defined maxima placed at about 75° between each other and each located at an angular distance of about 44° from the position of the 006 maximum. In some specimens (e.g., *P. maximus*, Fig. 7) some 104 pole maxima determined by conventional XRD texture analysis show an appreciably greater angular dispersion and even fuse. SEM-EBSD analyses (Fig. 8) make it possible to obtain a direct correlation between the actual crystallographic orientation determined from the Kokuchi patterns and the growth direction of crystals, determined from SEM images. It can be observed that the 001 maximum, the center of the diagram and one of the 104 maxima (the one in a more advanced position) are all aligned following the growth direction of folia.

4. Discussion

The foliated layer is the calcitic analogue of nacre in the sense that both biomaterials are composed of highly oriented platy crystals arranged in sheets. Unlike nacre, the crystallographic properties of the foliated layer are not so well understood and, as previously mentioned, in the literature we find contradictory reports about its organization. In this study we have applied different electron and X-ray diffraction techniques to study the foliated layer and determine its level of organization on different length scales.

The mode in which the foliated layer becomes organized can be inferred by studying this layer at different stages of development. We have observed how its secretion resumes on top of organic layers, produced after a refractory period of shell deposition. Initial deposits consist of isolated aggregates with irregular to pseudo-hexagonal outlines, constituted by co-oriented calcite laths; the subsequent fact that aggregates extend laterally and that their density increase causes them to impinge on each other. These aggregates resemble the inorganic calcite aggregates precipitated in the presence of a poly-acrylamide hydrogel by Grassmann et al. (2003), although they differ in the expressed crystal faces. At a short distance (a few hundred microns), the material becomes highly organized and displays a coherent crystallographic orientation (Fig. 5).

X-ray and electron diffraction analyses imply that the foliated layer is a highly ordered material consisting of crystals with their three main crystallographic axes aligned (that is, it has a sheet texture). The angles between 104 maxima of the pole figures (about 75°) and between those and the 001 maximum (44°) correspond to the angles between different $\{10\bar{1}4\}$ rhombohedral faces and to the angle between $\{0001\}$ and $\{10\bar{1}4\}$ faces (Fig. 3D) in a calcite crystal, respectively. The slight azimuthal disorder observed in several pole figures of *P. maximus* (Fig. 7) suggests that crystals are slightly rotated around the *c*-axis (turbostratic distribution). This may be attributed to the presence of co-existing sets of folia running in different directions (a fact usually observed by SEM).

Calcite crystals of the foliated layer are oriented with their *c*-axis tilted back (i.e., opposite to the growth direction) with respect to the shell surface normal (by some 21–30°). One of the $\{10\bar{1}4\}$ rhombohedral faces always looks in the direction of advance of the lath and the other two upper faces related by symmetry look backwards. This orientation has been consistently found in all eight species (which are representative of five families;

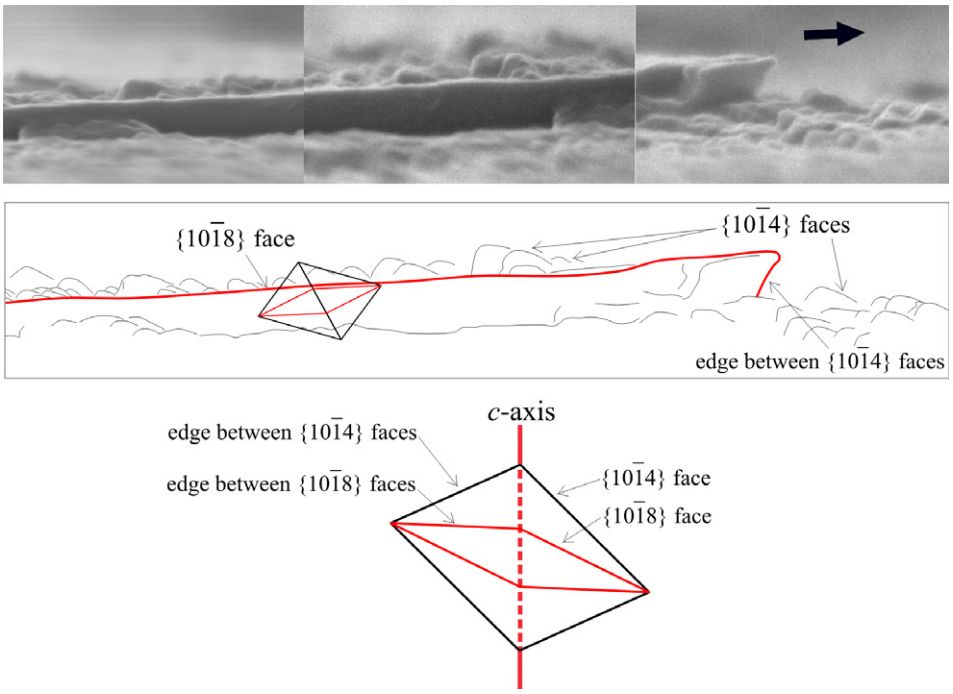

Fig. 9. Side view of a corroded lath, showing the outlines of corrosion rhombohedra. The lateral outline of the $\{10\bar{1}4\}$ calcite rhombohedron is fitted to the corrosion rhombohedra by tilting the *c*-axis opposite to the growth direction (arrow). Then, the outline of the $\{10\bar{1}8\}$ rhombohedron is coincident with the surface of the lath.

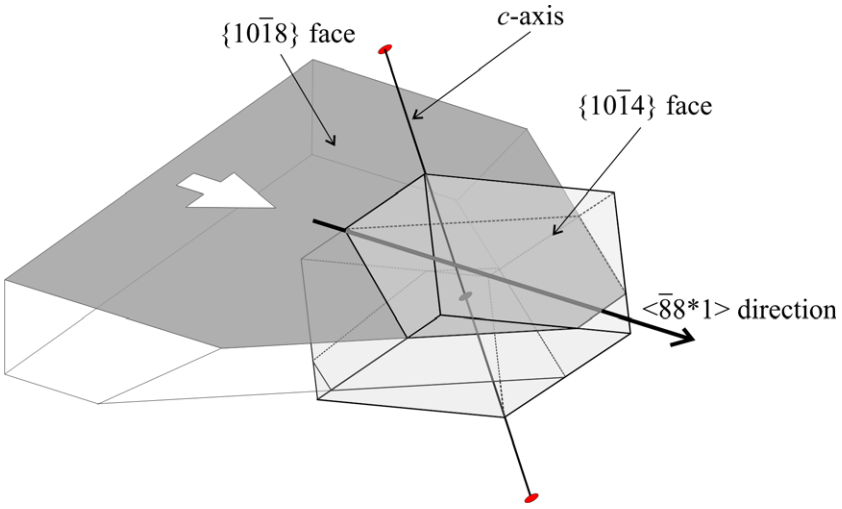

Fig. 10. Proposed model for the crystallography of the foliated layer, explained by showing the interpenetration of a lath with the $\{10\bar{1}4\}$ rhombohedron. The surface of the lath is a $\{10\bar{1}8\}$ face and contains an $\langle\bar{8}8*1\rangle$ direction, which is parallel to the growth direction (white arrow). There is a $\{10\bar{1}4\}$ face looking in the growth direction. Consequently, the *c*-axis is tilted opposite to this direction. In this example, the terminal faces of laths are $\{10\bar{1}4\}$ rhombohedral faces.

see Table 1) analysed either by XRD or EBSD (Figs. 7 and 8) and has been confirmed by SEM observations of naturally corroded specimens (Fig. 6). In these specimens the corroded crystals express $\{10\bar{1}4\}$ rhombohedral faces tilted so that the *c*-axis is inclined opposite to the growth direction of the folia (Fig. 9). In samples of *C. varia* and *Pr. jeffreysi*, terminal faces showing very good exposition are unequivocally $\{10\bar{1}4\}$ rhombohedral faces of calcite (Fig. 4B and C).

In our analyses the planes coinciding with the surface of folia are subparallel (typically at an angle of 2–3°) to the shell surface. Therefore, the poles associated to this plane would plot at a small distance of the center of the corresponding pole figure. The most likely centered face is a $\{10\bar{1}8\}$ rhombohedral face, which is at 26.3° of the $\{0001\}$ face (Fig. 3C and D). In fact, when the approximate positions of the 108 poles are plotted on pole figures (Figs. 7 and 8), there is always one such poles very close to

the center of the pole figure (the maximal deviation measured is 5°. A 108 pole figure derived from EBSD analyses is shown in Fig. 8 and it can be appreciated how a maximum is located centrally. Additionally, the inclination of $\{10\bar{1}4\}$ rhombohedral faces observed in corroded samples implies that one of the $\{10\bar{1}8\}$ faces is parallel to the lath surface (Fig. 9). The crystallographic model so far proposed is depicted in Fig. 10. In brief, crystals are preferentially oriented with a $\{10\bar{1}8\}$ crystal face parallel to the surface of the laths and a $\langle\bar{8}8*1\rangle$ direction aligned with the growth direction (Fig. 10).

We therefore agree with the conclusions of Taylor et al. (1969), and partly, with those of Runnegar (1984) that the lath surfaces are $\{10\bar{1}8\}$ rhombohedral faces (Fig. 2). Nevertheless, the former authors did not determine axial orientations, whereas, unlike us, Runnegar (1984) placed the *c*-axis inclined forward towards the direction of growth (his Type 2) or at 30° of it (Type 3). He came to the conclusion that the foliated microstructure of bivalves had three different crystallographic arrangements (Fig. 2) by taking the angle between the growing edges of laths as an additional distinctive criterion. In our opinion, based on the constancy of the distribution of pole maxima in the different groups analyzed, there is only one crystallographic orientation of calcite crystals in the foliated microstructure.

In biogenic calcite, the expression of faces other than the basal $\{0001\}$ face or the $\{10\bar{1}4\}$ cleavage rhombohedra results from their stabilization by preferential absorption of specific organic molecules (Addadi and Weiner, 1985). For example, in sea urchin spicules normally expressed faces are $\{hki0\}$ prismatic faces, which are parallel to the *c*-axis (e.g., Berman et al., 1993). The expressed $\{10\bar{1}8\}$ faces of calcite found in the surfaces of folia have neither been described in biomineral systems nor found in inorganically precipitated calcite crystals in which the negative $\{01\bar{1}8\}$ rhombohedra is expressed instead (e.g., "nail head" calcite; Kostov et al., 1999). Therefore, this type of face must be stabilized by particular molecules from the organic matrix.

5. Conclusions

The combined use of SEM, electron, and X-ray diffraction techniques provides complementary and highly detailed information about the organization of shell microstructures on different length scales.

The foliated layer is a highly ordered biomaterial with a very well defined crystallographic orientation which consistently displays the same characteristics in the different groups with this microstructure. Calcite crystals are oriented with their three main axes aligned. They have their *c*-axis tilted back relative to the shell normal (and the growth direction of folia) and have one of their $\{10\bar{1}8\}$ rhombohedral faces parallel to the lath surface. Further effort is necessary to define both the mechanisms inducing the expression of $\{10\bar{1}8\}$ crystallographic planes and that producing such a high degree of orientation of calcite crystals.

Acknowledgments

We thank Juan de Dios Bueno Pérez (CIC, Univ. Granada) for sample preparation, and Joaquín Ramírez and Francisco Varela Feria (CITIUS, Univ. Sevilla) for EBSD, and SEM operation. This study was supported by Research Projects CGL2004-00802 and REN2003-7375 (DGI, MCyT), and by the Research Groups RNM190 and RNM179 (CICE, JA).

References

Addadi, L., Weiner, S., 1985. Interactions between acidic proteins and crystals: stereochemical requirements in biomineralization. Proc. Natl. Acad. Sci. USA 82, 4110–4114.

Addadi, L., Weiner, S., 1992. Control and design principles in biological mineralization. Angew. Chem. 31, 153–169.

Beeston, B.E.P., Horne, R.W., Markham, R., 1986. Electron Diffraction and Optical Diffraction Techniques. North-Holland, Amsterdam.

Berg-Madsen, V., 1987. *Tuarangia* from Bornholm (Denmark) and similarities in Baltoscandian and Australasian late Middle Cambrian Faunas. Alcheringa 11, 245–259.

Berman, A., Hanson, J., Leiserowitz, L., Koetzle, T.F., Weiner, S., Addadi, L., 1993. Biological control of crystal texture: a widespread strategy for adapting crystal properties to function. Science 259, 776–779.

Carter, J.G., 1980. Guide to bivalve shell microstructures. In: Rhoads, D.C., Lutz, R.A. (Eds.), Skeletal Growth of Aquatic Organisms. Plenum Press, New York, pp. 645–673.

Carter, J.G., 1990. Chapter 10. Evolutionary significance of shell microstructures in the Palaeotaxodonta, Pteriomorphia and Isofilibranchia (Bivalvia: Mollusca). In: Carter, J.G. (Ed.), Skeletal Biomineralization: Patterns, Processes and Evolutionary Trends, vol. 1. Van Nostrand Reinhold, New York, pp. 135–296.

Carter, J.G., Hall, R.M., 1990. Polyplacophora, Scaphopoda, Archaeogastropoda and Paragastropoda (Mollusca). Plates 122–134. In: Carter, J.G. (Ed.), Skeletal Biomineralization: Patterns, Processes and Evolutionary Trends, Atlas and Index, vol. 2. Van Nostrand Reinhold, New York, pp. 29–51.

Chateigner, D., Hedegaard, C., Wenk, H.-R., 2000. Mollusc shell microstructures and crystallographic textures. J. Struct. Geol. 22, 1723–1735.

Grassmann, O., Neder, R.B., Putnis, A., Löbmann, P., 2003. Biomimetic control of crystal assembly by growth in an organic hydrogel network. Am. Mineral. 88, 647–652.

Kostov, I., Kostov, R., I., 1999. Crystal habits of minerals. Pensoft, Sofia.

MacKinnon, D.I., 1982. *Tuarangia paparua* n. gen. and n. sp., a late Middle Cambrian pelecypod from New Zealand. J. Paleontol. 56, 589–598.

Randle, V., 2000. Theoretical framework for electron backscattering diffraction. In: Schwartz, A.J., Kumar, M., Adams, B.L. (Eds.), Electron Backscatter Diffraction in Materials Science. Kluwer Academic, New York, pp. 19–30.

Randle, V., Engler, O., 2000. Introduction to Texture Analysis: Macrotexture, Microtexture and Orientation Mapping. Gordon and Breach Science, Amsterdam.

Rodríguez-Navarro, A.B., Gaines, K.F., Romanek, C.S., Masson, G.R., 2002. Mineralization of clapper rail eggshell from a contaminated salt marsh system. Arch. Environ. Con. Tox. 43, 449–460.

Runnegar, B., 1984. Crystallography of the foliated calcite shell layers of bivalve molluscs. Alcheringa 8, 273–290.

Runnegar, B., 1985. Shell microstructures of Cambrian molluscs replicated by phosphate. Alcheringa 9, 245–257.

Sykes, C.S., Wheeler, A.P., Wierzbicki, A., Mount, A.S., Dillaman, R.M., 2000. Nucleation and growth of calcite on native versus pyrolized oyster shell folia. Biol. Bull. 198, 50–66.

Taylor, P.D., Weedon, M.J., 2000. Skeletal ultrastructure and phylogeny of cyclostome bryozoans. Zool. J. Linn. Soc. Lond. 128, 337–399.

Taylor, J.D., Kennedy, W.J., Hall, A., 1969. Shell structure and mineralogy of the Bivalvia. Introduction. Nuculacae-Trigonacae. Bull. British Mus. Nat. Hist. Zool. 3 (Suppl.), 1–125.

Watabe, N., Wilbur, K.M., 1961. Studies on shell formation. IX. An electron microscope study of crystal layer formation in the oyster. J. Biophys. Biochem. Cy. 9, 761–771.

Watabe, N., Sharp, D.G., Wilbur, K.M., 1958. Studies on shell formation. VIII. Electron microscopy of crystal growth of the nacreous layer of the oyster *Crassostrea virginica*. J. Biophys. Biochem. Cy. 4, 281–286.

Williams, A., 1997. Shell structure. In: Kaesler, R.L. (Ed.), Treatise on Invertebrate Paleontology, Part H, Brachiopoda Revised. The Geological Society of America Inc., The University of Kansas, Boulder, Colorado, and Lawrence, KS, pp. 267–320.